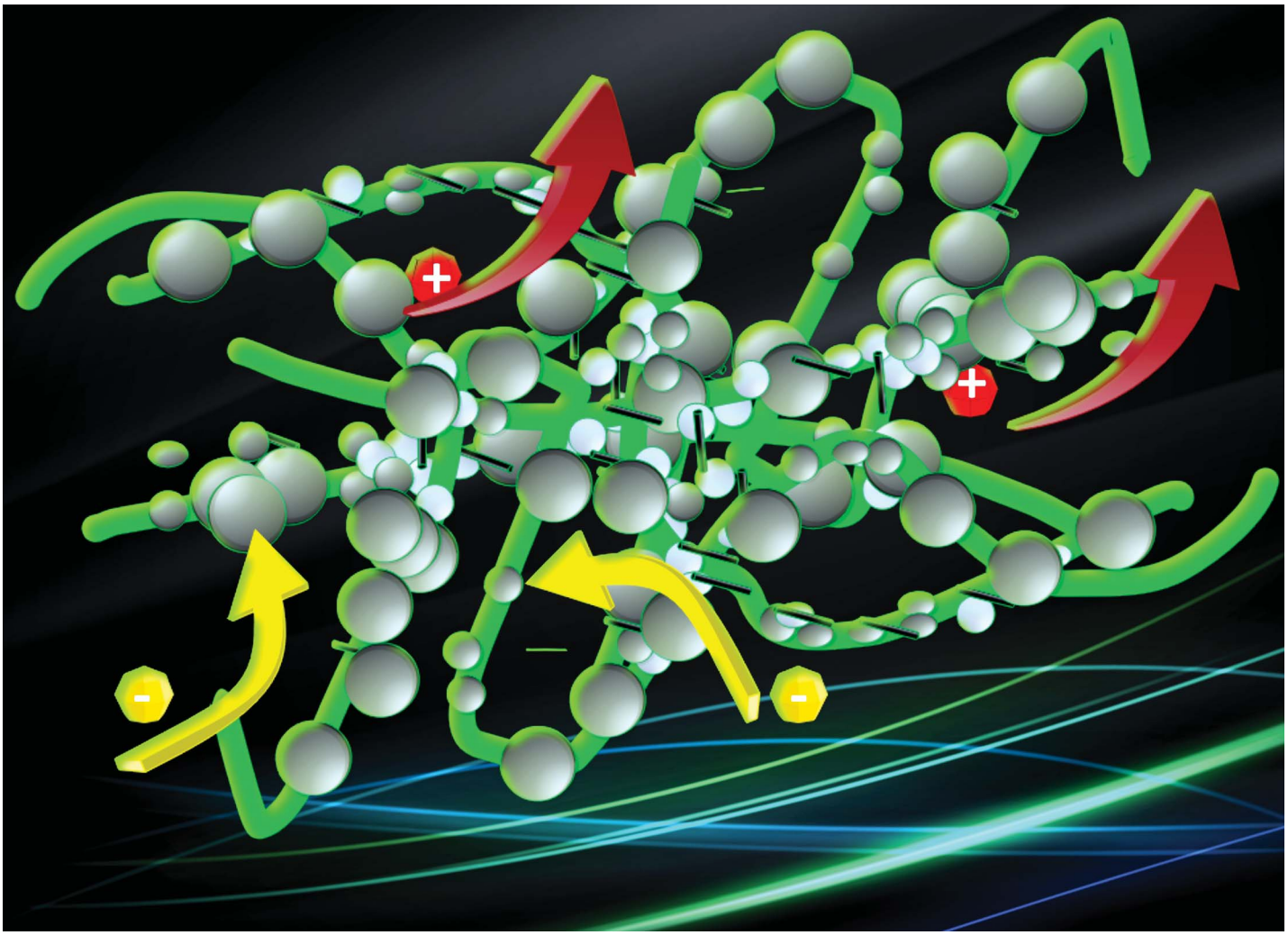

Demonstration of an effective way to utilize electrospinning and electrospraying to build 3D-hetero-nanoachitectures as high-performance electrodes for flexible energy storage by A/Prof. Shengyuan Yang and Prof. Meifang Zhu at the State Key Laboratory for Modification of Chemical Fibers and Polymer Materials (SKLFPM), Donghua University.

Controlled synergistic strategy to fabricate 3D-skeletal hetero-nanosponges with high performance for flexible energy storage applications

3D-heteronanosponges were inexpensively built from polyindole conducting polymer and carbon nanotubes via controlled electrospinning/electrospraying nozzle spacing. The flexible electrodes with 3D-skeletal nanostructures made up of nanofibers, nanotubes, and nanoparticles as active building blocks provided shortened ion diffusion paths with capability to exploit the extra third dimension unlike traditional 2D thin materials.

As featured in:

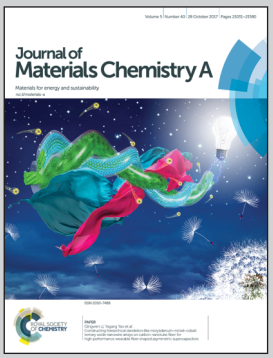

See Shengyuan Yang, Meifang Zhu *et al.*, *J. Mater. Chem. A*, 2017, **5**, 21114.

ROYAL SOCIETY OF CHEMISTRY

rsc.li/materials-a

Registered charity number: 207890

Journal of Materials Chemistry A

COMMUNICATION

View Article Online
View Journal | View Issue

Cite this: J. Mater. Chem. A, 2017, 5, 21114

Received 17th July 2017
Accepted 8th August 2017

DOI: 10.1039/c7ta06242g

rsc.li/materials-a

Controlled synergistic strategy to fabricate 3D-skeletal hetero-nanosponges with high performance for flexible energy storage applications†

Mike Tebyetekerwa,[a] Xingping Wang,[a] Yongzhi Wu,[b] Shengyuan Yang,*[a] Meifang Zhu*[a] and Seeram Ramakrishna[c]

The simple combination of electrospinning and electrospraying has previously been studied by some researchers to fabricate novel nanomaterials for energy applications in batteries and supercapacitors. However, the performance of the resultant materials (especially electrodes) is not sufficient despite the collaboration of these two boundless methods. Herein, we report the best approach towards effective synergistic control of the two techniques to improve the electrochemical performance of the resultant electrode materials. Interestingly, the reported modified technique yielded unusual 3D-skeletal architectures with dissimilar but remarkable capacitance values. The current methodology is an easy and inexpensive approach to realizing 3D high-performance electroactive materials.

The anticipated flexible and wearable smart energy devices in next generation electronics have triggered new advanced requirements in materials that build up these devices.[1] Flexibility and electroactivity, with high energy and power density are some of the demands. In this line, therefore, many different materials design approaches have been devised in order to fulfil the needs. To be able to do this, researchers have either modified traditional fabrication techniques, combined different existing methods, and/or in other instances introduced entirely new fabrication approaches.[2–6] Electrospraying and electrospinning are among the fabrication techniques widely studied and modified. These two specific methods are known to provide novel, nanostructured and electroactive materials with the help of high electric fields. In electrospinning, nanofibers are formed from polymer solution as a result of high electric repulsion forces, whereas during electrospraying, nanoparticles are directly deposited onto a collector with the help of an electric force. Both of these techniques result in electrode materials with a range of morphologies such as nanofibers, nanotubes, nanoparticles, nanospheres and all other related domains, without any additional binder requirements.[7–9]

Recently, electrospinning and electrospraying techniques have been simply combined to provide advanced materials with unique properties and functions. These materials have found applications in energy storage such as in battery electrodes,[10–13] supercapacitor electrodes[14,15] and separators.[16–18] However, despite this synergistic approach, only straightforward and traditional assembly has been previously employed. In all of the previous works, it was more like an assembly of individual electrospinning and electrospraying nozzles to obtain the new materials. In this work, our aim was to break the routine so as to produce better materials with high performance. We employed the conducting polymer polyindole (Pind), which is one of the least studied conducting polymers but has promising functions, and carbon nanotubes (CNTs) with the aim of setting the bar for our proposed modified fabrication synergistic technique. We show the most effective and efficient way to utilize the two combined methods of electrospinning and electrospraying by controlling the spacing between the two nozzles.

Generally, previously reported Pind capacitance values have been low.[19,20] Better performance was only achieved with other nanomaterials such as transition metal oxides,[21] carbon-based materials,[20,22,23] and/or a combination of both.[24,25] The capacitance behavior of conducting polymers (CPs) is known to be highly dictated by the morphology, surface area and porosity,[26–29] which all depend on the fabrication approach. Pind and Pind-based nanocomposite materials for supercapacitor electrodes previously reported were all slurry-based, where a pile of active materials were deposited onto current collectors.[19,20,22–25] For example, Mudila *et al.*[20] reported Pind/graphene oxide (GO) nanocomposites synthesized by *in situ* polymerization. The resultant Pind/GO electrode gave a specific capacitance of only 399.97 F g^{-1}. Following the same

[a]State Key Laboratory for Modification of Chemical Fibers and Polymer Materials, College of Material Science and Engineering, Donghua University, Shanghai 201620, P. R. China. E-mail: cmseysy@dhu.edu.cn; zhumf@dhu.edu.cn

[b]Department of Information Science and Electronics Engineering, Zhejiang University, Hangzhou 310027, China

[c]Centre for Nanofibers and Nanotechnology, National University of Singapore, Singapore 117581, Singapore

† Electronic supplementary information (ESI) available. See DOI: 10.1039/c7ta06242g

conventional fabrication route, in 2016, other researchers employed Pind/CNT (206 F g^{-1}),[19] Pind/reduced GO(RGO) (322.8 F g^{-1}),[22] and Pind/PEDOT:PSS/carbon cloth (CC) (623 F g^{-1})[30] nanocomposites. Recently Wang *et al.*[23] also reported Pind/CNT/RGO, and their resultant electrodes gave a specific capacitance of only 383 F g^{-1} at 1.0 A g^{-1}. Other capacitance improvements have been reported but with the addition of more species of active materials such as Pind/V_2O_5/CC[25] and Pind/CNT/Co_3O_4 (ref. 24), which gave competitive specific capacitance values of 535 F g^{-1} and 442 F g^{-1} at 1.0 A g^{-1}, respectively. On a side note, exceptional values as high as 1805 F g^{-1} at 2.0 A g^{-1} were reported when Pind was used together with Co_3O_4, owing to the high capacitance of Co_3O_4.[21] Nanotechnology and controlled synthesis of nanostructured materials can be thought of as the answers to the observed previous quandary.

Herein, we report the controlled fabrication of Pind/CNT 3D-skeletal hetero-nanosponges (Pind/CNT NS) with unusual architectures as electrode active materials, which were obtained *via* simultaneous electrospinning and electrospraying. Diverging from the simple routine of electrospraying and electrospinning, to get the best out of the techniques, for the first time, we critically focused our attention on the effect of controlled spacing of the electrospraying and electrospinning nozzles on the performance of electrode materials. 3D architectures have recently starred as the ideal structures for energy storage in batteries[31] and supercapacitors.[27,28,32] This is ascribed to their ability to use the extra dimension compared to 2D architectures materials regarding charge storage. However, building such unique designs previously has been ultimately complex. Commonly known techniques for building 3D structured electrodes such as interdigitated structures rely on etching, modified layer-by-layer self-assembly, synergistic freeze-casting and sol–gel processes and 3D printing techniques.[33–38] In this work we provide a very cheap and inexpensive route, and the best way to realize 3D nanostructured architectures by using the two widely known boundless techniques of electrospinning and electrospraying.

To fabricate the Pind/CNT NS, special customized homemade electrospinning/electrospraying equipment was employed (Fig. S1a†). The electrospraying and electrospinning solutions were placed in different 15 ml syringes fitted with 20-gauge nozzles, each provided with a pump capable of driving it at 0.5 ml h^{-1} and 1.0 ml h^{-1}, respectively. The 20-gauge nozzle tips were tightly equipped with tubular connectors responsible for delivering the solutions to the high voltage region through the nozzles spaced at a distance (d = 4 cm, 8 cm and 12 cm) as shown in Fig. 1a. The electrospraying and electrospinning nozzles were 23-gauge and 22-gauge, respectively. An aluminum collector was placed at a distance of exactly 15 cm. Finally a high voltage of 20 kV was applied. Fig. 1b shows the effective area of the active materials which was considered for characterization and electrochemical analysis. Regarding the nozzle gauges employed, the 20-gauge nozzle was required to tightly fit the tubular connections to the solutions syringe (see Fig. S1b†). The nozzles of great concern were the 22-gauge and 23-gauge nozzles. Nanomaterials obtained *via* electrospinning, for

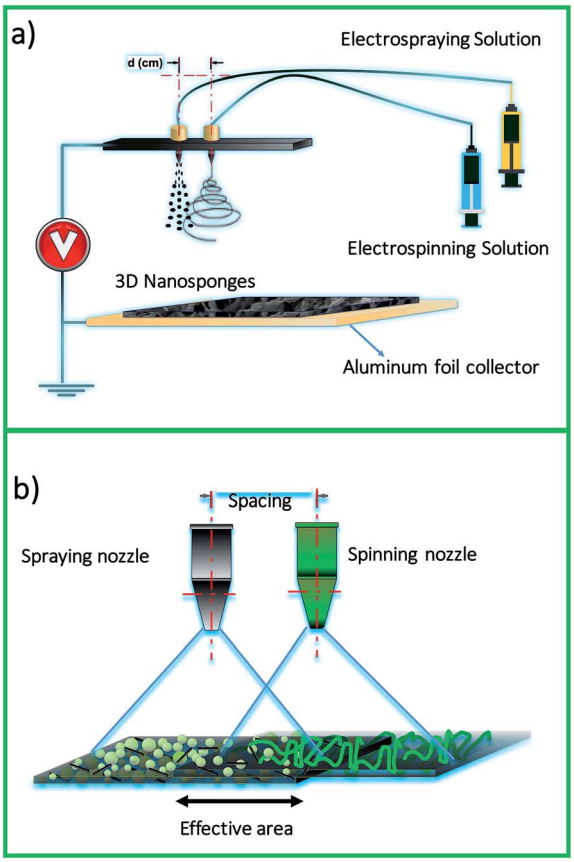

Fig. 1 (a) Schematic showing the fabrication of 3D hetero-nanosponges with d (cm) as the spacing between the nozzles and (b) the considered effective area.

example nanofibers and nanoparticles, are greatly influenced by the operational parameters of which nozzle gauge is among them. The nozzle diameters are responsible for the optimization of the force applied to the nozzles by the pumps. Therefore, the nozzle diameters significantly control the mass output of the electrospinning and electrospraying solutions being delivered to the high voltage region. When the Pind polymer solution was carefully optimized for electrospinning, for example, in this case *via* 22-gauge nozzles, fibers with diameters in the range of nanofibers could be easily obtained. The general rule follows that the smaller the spinning nozzle, the thinner the fibers. We note that with a 23-gauge nozzle, Pind nanofibers could not be achieved. Nanofibers of Pind, as previously reported in our work, could be optimally fabricated with a 22-gauge nozzle together with the earlier mentioned parameters.[39] With a 23-gauge nozzle, electrospraying would occur. For successful electrospraying, a low rate of solution flow and a high electrical conductivity value of the electrospray solution are required.[40] Therefore, increasing the nozzle gauge apparently decreased the flow rate (together with a reduction in the pump speed to 0.5 ml h^{-1}) coupled with CNT doping, and the solution conductivity was substantially increased which preferably resulted in electrospray materials interfaces. At the decreased flow rate of 0.5 ml h^{-1}, the electrical field was strong enough to

break down the Pind/CNT/PEO composite. Therefore, summing up the experimental setup, nanoparticles, nanotubes (of CNTs) and nanofibers could be simultaneously collected on the same collector which as a result provided novel materials with new functionalities.

Morphology is a critical material property which significantly affects overall performance especially with regards to energy storage applications.[28] Therefore a controllable approach to realize special material morphologies is a major topic of concern for material scientists today. The surface Scanning Electron Microscope (SEM) images (Fig. 2a–c) and cross-section SEM images (Fig. 2d–f) of various fabricated Pind/CNT NS are provided together with corresponding schematic visualizations in Fig. 2g–i (obtained using a SEM, Hitachi S-4800N). The SEM images revealed unique morphologies with great differences at the nanoscale level. The Pind/CNT NSs obtained with nozzle spacings of 4 cm, 8 cm and 12 cm will be denoted Pind/CNT NS-4, Pind/CNT NS-8, and Pind/CNT NS-12, respectively, henceforth for ease. From the surface SEM, it can be observed that all of the Pind/CNT NSs were dotted with nanostructured CNTs and nanoparticles of Pind together with fibrous morphology. The fibrous morphology is attributed to the electrospinning, whereas the Pind nanoparticles and CNTs are attributed to the electrospraying. The surface morphology of Pind/CNT NS-4 (Fig. 2a) was more perturbed, which is ascribed to the decreased spacing between the electrospraying and electrospinning nozzles resulting in maximum interference of the electrospinning jet trajectories by the electrospray particles. Also, prevailing fibers could be observed which had very fine diameters which is due to the high total area voltage around both nozzles causing increased orientation.[41] This can also explain why the prevailing fibers' diameters were seen to increase as the nozzle spacing increased (compare insets in Fig. 2a–c), because of less spinning jet interference. For the Pind/CNT NS-8 a distinct fibrous morphology with moderate interference (Fig. 2b) and a 3D "bread-like" cross-section (Fig. 2e) was observed. Further still, the Pind/CNT NS-12 (Fig. 2c) morphology was almost fine with little nanoparticles due to the increased nozzle spacing. In a nutshell, the resultant Pind/CNT NS depicted interconnected, skeletal and fibrous 3D

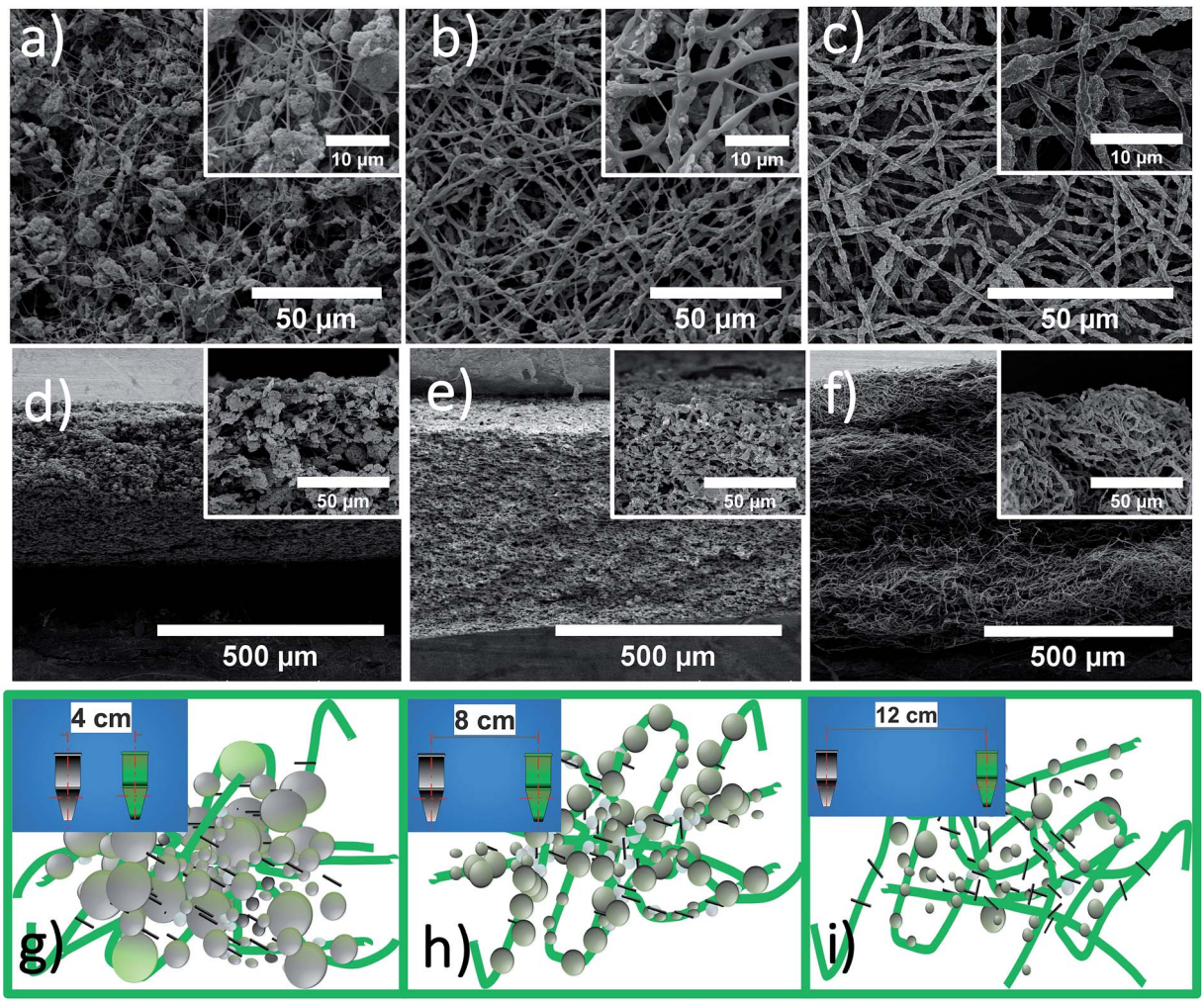

Fig. 2 SEM analysis. Surface and cross-sectional SEM images of Pind/CNT NS-4 (a and d), Pind/CNT NS-8 (b and e) and Pind/CNT NS-12 (c and f). Insets are their magnifications. Proposed schematic visualizations of Pind/CNT NS-4 (g), Pind/CNT NS-8 (h) and Pind/CNT NS-12 (i).

morphologies fitting electrode applications in supercapacitors. Such hetero-nanoarchitecture arrangements are known to present shorter diffusion paths for electronic drive within the materials, and hence high charge–discharge rates favorable in supercapacitors.[27] We note that the proposed approach could fabricate 3D-skeletal structures with much ease compared to the 3D-interdigitated structures fabricated by numerous and complex traditional microelectromechanical system processing procedures,[34,36] modified layer-by-layer self-assembly,[33,37] synergistic freeze-casting and sol–gel processes[35,38] and 3D printing techniques.[35]

SEM images alone cannot provide the full information about the constituent components within the fabricated hetero-nanosponges. Therefore, we conducted characteristic element image mapping with an energy dispersive spectrometer (EDS, Bruker, XFlash660) to view the constituents. EDS surface element analysis highlighted the presence of three major elements as expected (Fig. 3). It can be observed that carbon (C), oxygen (O), and nitrogen (N) were the main element constituents. It is evident from the maps that carbon was more and widely distributed compared to other elements due to the presence of CNTs in the nanocomposites. The presence of oxygen and nitrogen further confirmed the distribution of Pind polymer nanoparticles throughout the hetero-nanostructures.

The electrochemical behavior of the Pind/CNT NSs was standard tested with Cyclic Voltammetry (CV), Galvanostatic Charge Discharge (GCD) and Electrochemical Impedance Spectroscopy (EIS) in the three-electrode setup using an electrochemical workstation (CHI 660E) in 1 M H_2SO_4. The Pind/CNT NS acted as the working electrode, Ag/AgCl (Metrohm, 3.5 M KCl) as the reference electrode, and platinum thin wire as the counter electrode. The mass of the active material directly controlled by monitoring the experimental time was made to lie between 2.0–2.6 mg. Fig. 4a shows the typical CV curves obtained at a scan rate of 20 mV s^{-1} for the Pind/CNT NS fabricated at varying nozzle spacings (for individual CV curves at different scan rates see Fig. 4b, S3a and S4a†). Distinct differences were observed in the Pind/CNT NS-12 CV due to the presence of fewer CNTs in the effective active materials caused by the increased nozzle spacing. These CV curves at 20 mV s^{-1} gave specific capacitance values of 365 F g^{-1}, 442 F g^{-1} and 322 F g^{-1} for Pind/CNT NS-4, Pind/CNT NS-8, and Pind/CNT NS-12, respectively. The two redox peaks observed in the CV curves are associated with the typical redox reactions of Pind and also the

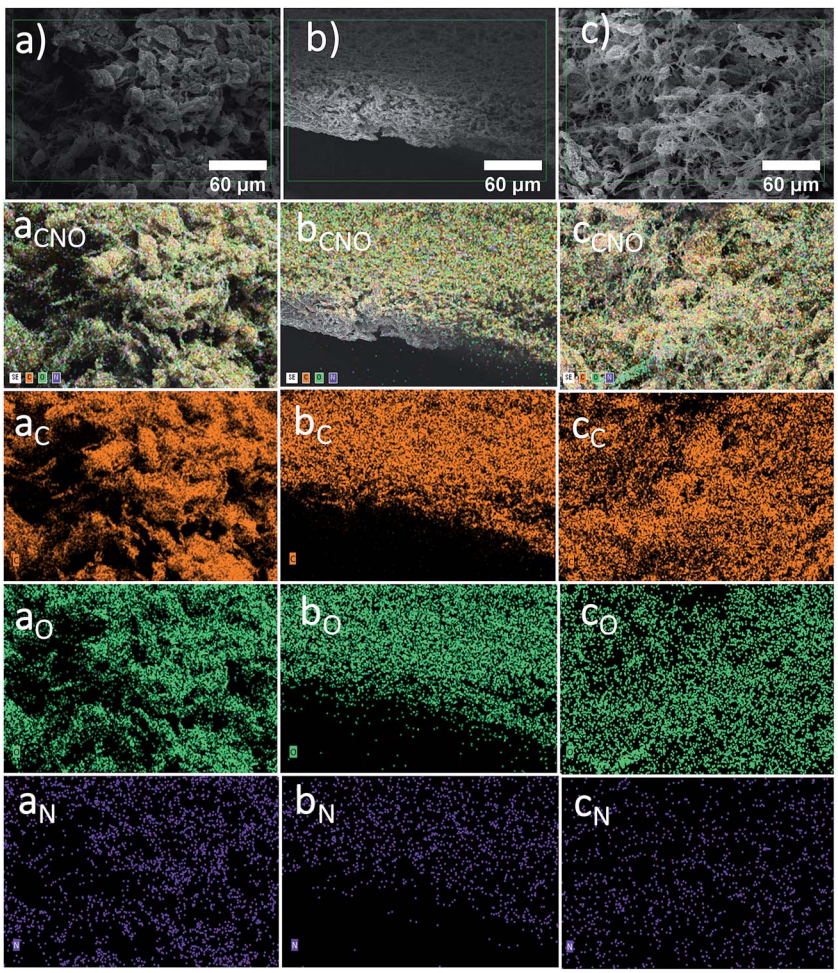

Fig. 3 Cross-section EDS elemental mapping of Pind/CNT NSs. (a) Pind/CNT NS-4, (b) Pind/CNT NS-8 and (c) Pind/CNT NS-12. As an example, a_C is carbon, a_O is oxygen and a_N is nitrogen for Pind/CNT NS-4 in (a).

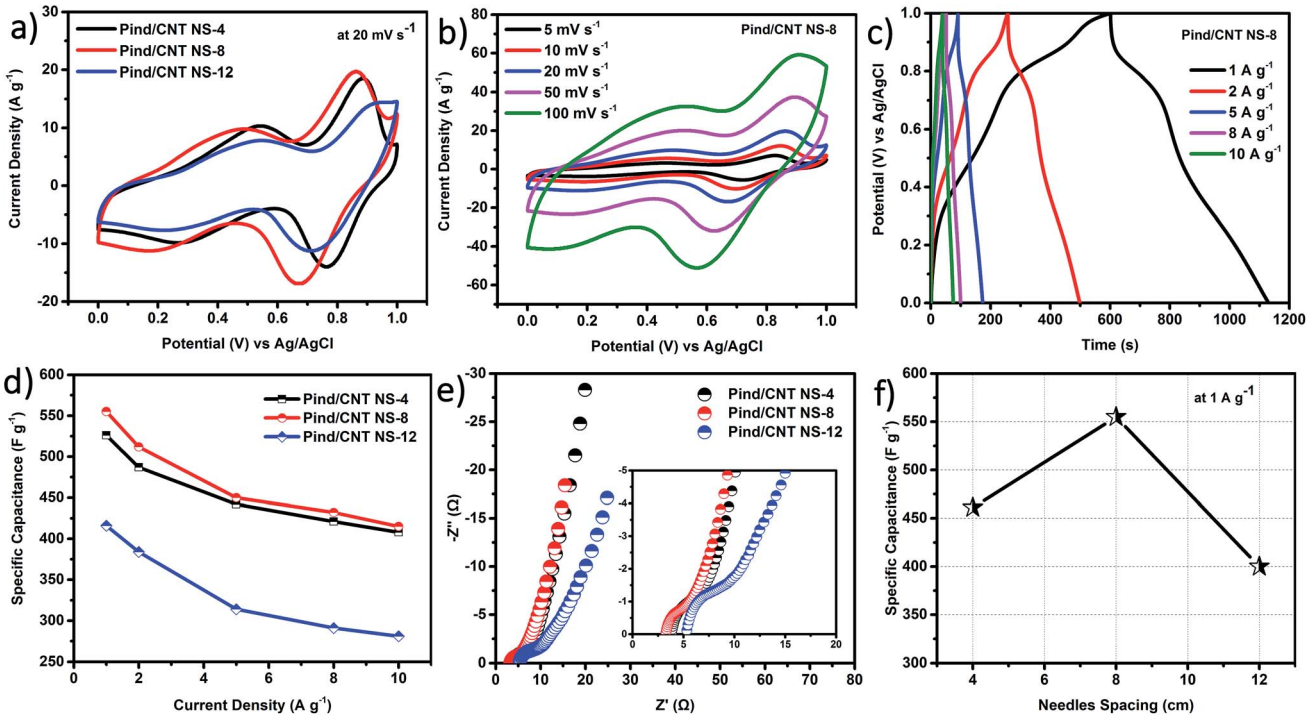

Fig. 4 Electrochemical performance of Pind/CNT NSs. (a) CV curves of Pind/CNT NS-4, Pind/CNT NS-8, and Pind/CNT NS-12 at 20 mV s^{-1}, (b) CV curves and (c) GCD curves of Pind/CNT NS-8, (d) the specific capacitance rate retention of the electrodes at varying current densities, (e) a Nyquist plot of the Pind/CNT NS (inset is the zoom in the higher-frequency region) and (f) variation of specific capacitance with the nozzle spacing at a current density of 1 A g^{-1}

transition between the quinone/hydroquinone states of CNTs with oxygen containing groups.[30,42] The specific capacitance values for Pind/CNT NS-4, Pind/CNT NS-8, and Pind/CNT NS-12 were as high as 461 F g^{-1}, 555 F g^{-1}, and 400 F g^{-1}at 1.0 A g^{-1}, obtained from Fig. S3b, 4c and S4b,† respectively. Generally, the capacitance increased in the order of Pind/CNT NS-8 > Pind/CNT NS-4 > Pind/CNT NS-12 as depicted in Fig. 4d and f. To explain this trend, it is crucial to first understand the fabrication process and the arrangement of the nozzles with their individual solutions involved. Herein, the electrospinning syringe was filled with Pind in PEO solution whereas the electrospraying syringe had Pind, CNTs and PEO solution (for details see the Experimental section in the ESI†). The effective area analyzed (see Fig. 1b) and the Equivalent Series Resistance (ESR) values of the respective electrodes, which were the values of (Z_{Real}) of impedance at 1 kHz frequency from EIS (Fig. 4e),[43] were considered. The electrodes gave different but low ESR values of 4.79 Ω, 5.68 Ω and 8.65 Ω for Pind/CNT NS-8, Pind/CNT NS-4, and Pind/CNT NS-12, respectively. These values represent the hetero-nanostructured materials' electronic DC resistance, not including any ionic contributions. Therefore, the skeletal structures had excellent connections within and throughout their architectures. These obtained skeletal structures provided controlled arrangement of nanofibers, nanotubes, and nanoparticles as active materials/building blocks and thus an improved specific surface area, which significantly provided adequate contact with the electrolyte. Similar results were also observed when nanosheets were employed as building blocks for such 3D nanostructures.[28]

To explain the earlier mentioned ESR value differences and trend (obtained from Fig. 4e), the SEM images and schematic visualizations provided in Fig. 2 can be employed. The CNTs within the skeletal electrodes are believed to have greatly influenced the conductivity of the materials owing to their known high conductivity.[44] As Pind is poorly conducting, when composited with PEO polymer to form nanofibers *via* the electrospinning nozzle it only could not give good capacitance values. However, the presence of some CNTs due to the electrospraying jets played a significant role in conductivity bridging within the PEO polymer areas in the nanofibers. This was true especially in Pind/CNT NS-8 whose morphology had a good arrangement of nanofibers with electrospray particles dotted all around them, enabling continuous current transfer. Thus, the Pind/CNT NS-8 electrode showed the best energy storage performance, which was attributed to the optimized arrangement of building materials (at the nanoscale) and good electrical conductivity due to the presence of CNTs. The addition of CNTs to active materials is known to improve the electrical conductivity of the electrode and hence enables longer discharge times with lower ESR values, as previously reported even for transition metal composites.[29] On the contrary, for Pind/CNT NS-4, though its ESR was better than that of Pind/CNT NS-12 with a connected network of nanofibers, it was inferior to that of Pind/CNT NS-8. This is because it lacked a connected network of dense nanofibers, but had more Pind

and CNTs from the electrospraying nozzle within the effective area, and the CNTs boosted its conductivity. The opposite is true for Pind/CNT NS-12, which had a finely connected network of nanofibers but fewer materials from electrospraying due to the increased spacing between the electrospraying and electrospinning nozzles. The CV and GCD curves of Pind/CNT NS-8 are provided in Fig. 4b and c, respectively, as their resultant electrodes demonstrated the best capacitive behavior. The CV curves are seen to have considerable areas and cyclic stability even at a high scan rate of 100 mV s^{-1} within a 1 V window, indicating good performance. Overall, the excellent electrochemical behavior of the NS reported is attributed to the 3D-skeletal morphology of the electrode materials. Still, electronic conductivity and ionic conductivity of electrode materials contribute significantly to the electrochemical properties of materials.[2,27–29]

The calculated capacitance values of the Pind/CNT NSs were further compared with their current densities as shown in Fig. 4d. Generally, the capacitance was observed to decrease with increasing current density due to the fact that the diffusion of dopants during Pind's redox process is a rate determining step.[39] Therefore, lowering the charge/discharge current readily allows a good number of dopant ions to flow in/out of Pind, which translates into increased capacitance values with decreased current density.[39,45] However, to be specific, Pind/CNT NS-8, Pind/CNT NS-4, and Pind/CNT NS-12 showed excellent rate retentions of 74.5%, 61.38%, and 55%, respectively (1–10 A g^{-1}). These values are better than those of Pind/carbon slurry-based nanomaterials in the literature, which is attributed to the 3D hetero-nanostructures of the reported composites[19,20,22] with relatively low ESR values and various nanopores, which acted as unobstructed channels for the diffusion of electrolyte ions.

Fig. 5a shows the cycling stability test of the Pind/CNT NS electrode materials at a scan rate of 20 mV s^{-1}. Interestingly, the Pind/CNT NS-4 electrodes showed the best capacitance retention of 97.8% (after 2000 cycles) which is attributed to its dense 3D non-uniform morphology, capable of holding together the active materials in the form of non-uniform entanglements, and limiting over swelling and the resultant shrinkage caused by charge–discharge currents. The better uniformity kills the capacitance retention of the NS as the active materials are susceptible to expansions and contractions during charge–discharge as in Pind/CNT NS-8 and Pind/CNT NS-12. However, Pind/CNT NS-8 and Pind/CNT NS-12 also showed reasonably good cycle retention abilities of 96.9% and 93.8%, respectively, after 2000 cycles, which were better values than those of Pind/CNT[19] and Pind/RGO[22] in the previous literature. The observed good cycle retention can be attributed to the layer by layer like assembly of the active materials, but with secure fixation to each other.[33] This is because the different materials from the spinning and spraying nozzles adhered to each other within the electrodes, with PEO improving their adhesion within the nanostructures. The specific capacitance values reported in this communication are better than previous ones in the literature for slurry-based Pind/CNT (206 F g^{-1}),[19] Pind/RGO (322.8 F g^{-1}),[22] Pind/CNT/RGO(383 F g^{-1}),[23] Pind/GO(399.97 F g^{-1})[20] and Co_3O_4/Pind/CNT (442.5 F g^{-1}),[24] as depicted in Fig. 5b. This is mainly due to two primary reasons: (1) the 3D active structure, capable of exploiting the third dimension for energy storage unlike traditional 2D materials[33] and (2) the nanofibers' electroactive structure, capable of introducing new reaction sites not easily obtainable in bulk materials, for example, the decreased pathways of charge transport.[46] Note that this work provides a facile and effective way to build and utilize the two synergistic techniques of electrospinning and electrospraying, which are capable of building 3D highly electroactive materials that readily present a higher gain area factor than 2D materials.[33]

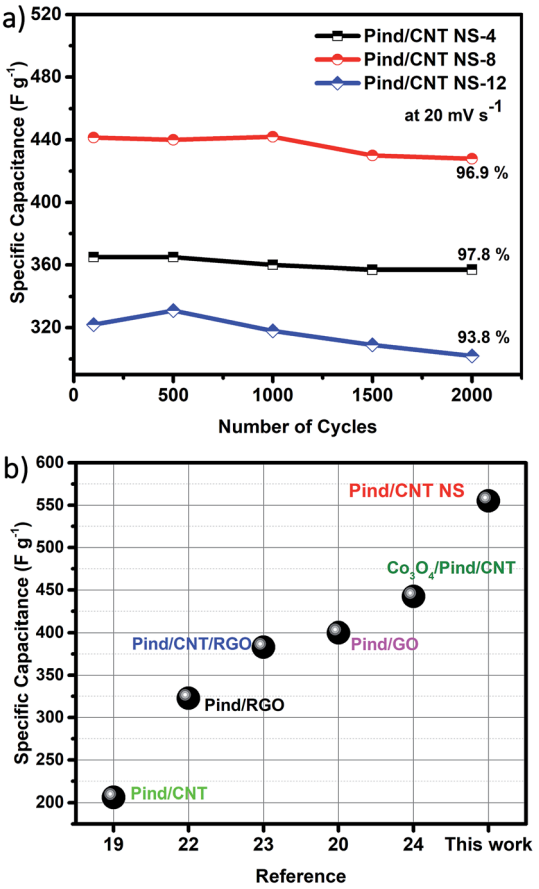

Fig. 5 (a) Capacitance retention of the electrodes after 2000 cycles and (b) comparison of the current work with previous reported Pind/carbon-slurry based nanocomposites.

In summary, we have demonstrated the best way to utilize the synergistic techniques of electrospraying and electrospinning by controlling the nozzle spacing. The approach gave remarkable improvements in the resulting materials' electrochemical properties, which is attributed to the 3D-skeletal morphology of the electrodes. The recorded improvements in the employed Pind/CNT capacitance values can be even further improved by employing transition metal oxides (such as V_2O_5, Co_3O_4, and MnO_2), conducting nanostructured metal materials (such as copper nanospheres), and adding a higher percentage of carbon-based materials to Pind. Furthermore, this approach can also be employed to obtain electrodes with 3D-skeletal

morphologies of other electroactive materials, with high-performance, at a lower cost, and with ease and scalability assured.

Conflicts of interest

There are no conflicts to declare.

Acknowledgements

The authors are grateful for the funds from the "Chenguang Program" supported by the Shanghai Education Development Foundation, Shanghai Municipal Education Commission (15CG32), the Fundamental Research Funds for the Central Universities (2232015D3-20), the Science and Technology Commission of Shanghai Municipality (16JC1400700), the National Natural Science Foundation of China (51673088) and the Program for Innovative Research Team in University of Ministry of Education of China (IRT_16R13).

Notes and references

1 W. Liu, M.-S. Song, B. Kong and Y. Cui, *Adv. Mater.*, 2017, **29**, 1603436.
2 X. Lu, C. Wang, F. Favier and N. Pinna, *Adv. Energy Mater.*, 2017, **7**, 1601301.
3 S. E. Moosavifard, M. F. El-Kady, M. S. Rahmanifar, R. B. Kaner and M. F. Mousavi, *ACS Appl. Mater. Interfaces*, 2015, **7**, 4851–4860.
4 J. A. Lee, M. K. Shin, S. H. Kim, H. U. Cho, G. M. Spinks, G. G. Wallace, M. D. Lima, X. Lepró, M. E. Kozlov and R. H. Baughman, *Nat. Commun.*, 2013, **4**, 1970.
5 S. Chen, W. Ma, Y. Cheng, Z. Weng, B. Sun, L. Wang, W. Chen, F. Li, M. Zhu and H.-M. Cheng, *Nano Energy*, 2015, **15**, 642–653.
6 W. Ma, S. Chen, S. Yang, W. Chen, Y. Cheng, Y. Guo, S. Peng, S. Ramakrishna and M. Zhu, *J. Power Sources*, 2016, **306**, 481–488.
7 D. Li and Y. N. Xia, *Adv. Mater.*, 2004, **16**, 1151–1170.
8 A. Greiner and J. H. Wendorff, *Angew. Chem., Int. Ed.*, 2007, **46**, 5670–5703.
9 L. Fei, S. H. Yoo, R. A. R. Villamayor, B. P. Williams, S. Y. Gong, S. Park, K. Shin and Y. L. Joo, *ACS Appl. Mater. Interfaces*, 2017, **9**, 9738–9746.
10 Y. Xu, Y. Zhu, F. Han, C. Luo and C. Wang, *Adv. Energy Mater.*, 2015, **5**, 1400753.
11 J. H. Lee, J.-M. Kim, J.-H. Kim, Y.-R. Jang, J. A. Kim, S.-H. Yeon and S.-Y. Lee, *Adv. Mater. Interfaces*, 2016, **3**, 1600173.
12 T. Yu, B. Lin, Q. Li, X. Wang, W. Qu, S. Zhang and C. Deng, *Phys. Chem. Chem. Phys.*, 2016, **18**, 26933–26941.
13 J.-M. Kim, C.-H. Park, Q. Wu and S.-Y. Lee, *Adv. Energy Mater.*, 2016, **6**, 1501594.
14 A. Tolosa, B. Krüner, N. Jäckel, M. Aslan, C. Vakifahmetoglu and V. Presser, *J. Power Sources*, 2016, **313**, 178–188.
15 J. H. Lee, J. A. Kim, J.-M. Kim, S.-Y. Lee, S.-H. Yeon and S.-Y. Lee, *Sci. Rep.*, 2017, **7**, 41708.
16 M. Yanilmaz, Y. Lu, M. Dirican, K. Fu and X. Zhang, *J. Membr. Sci.*, 2014, **456**, 57–65.
17 J.-H. Kim, J.-H. Kim, J.-M. Kim, Y.-G. Lee and S.-Y. Lee, *Adv. Energy Mater.*, 2015, **5**, 1500954.
18 Y.-S. Oh, G. Y. Jung, J.-H. Kim, J.-H. Kim, S. H. Kim, S. K. Kwak and S.-Y. Lee, *Adv. Funct. Mater.*, 2016, **26**, 7074–7083.
19 R. Oraon, A. De Adhikari, S. K. Tiwari, S. Bhattacharyya and G. C. Nayak, *RSC Adv.*, 2016, **6**, 64271–64284.
20 H. Mudila, S. Rana, M. Zaidi and S. Alam, *Fullerenes, Nanotubes, Carbon Nanostruct.*, 2015, **23**, 20–26.
21 R. P. Raj, P. Ragupathy and S. Mohan, *J. Mater. Chem. A*, 2015, **3**, 24338–24348.
22 Q. Zhou, D. Zhu, X. Ma, J. Xu, W. Zhou and F. Zhao, *RSC Adv.*, 2016, **6**, 29840–29847.
23 W. Wang and S. Wu, *Appl. Surf. Sci.*, 2017, **396**, 1360–1367.
24 X. Zhou, A. Wang, Y. Pan, C. Yu, Y. Zou, Y. Zhou, Q. Chen and S. Wu, *J. Mater. Chem. A*, 2015, **3**, 13011–13015.
25 X. Zhou, Q. Chen, A. Wang, J. Xu, S. Wu and J. Shen, *ACS Appl. Mater. Interfaces*, 2016, **8**, 3776–3783.
26 X. Lu, C. Wang, F. Favier and N. Pinna, *Adv. Energy Mater.*, 2016.
27 W. Wei, L. Mi, Y. Gao, Z. Zheng, W. Chen and X. Guan, *Chem. Mater.*, 2014, **26**, 3418–3426.
28 W. Wei, L. Mi, S. Cui, B. Wang and W. Chen, *ACS Sustainable Chem. Eng.*, 2015, **3**, 2777–2785.
29 W. Wei, W. Chen, L. Ding, S. Cui and L. Mi, *Nano Res.*, 2017, DOI: 10.1007/s12274-017-1586-3.
30 Q. Zhou, D. Zhu, X. Ma, D. Mo, F. Jiang, J. Xu and W. Zhou, *Electrochim. Acta*, 2016, **212**, 662–670.
31 J. W. Long, B. Dunn, D. R. Rolison and H. S. White, *Chem. Rev.*, 2004, **104**, 4463–4492.
32 M. Beidaghi and Y. Gogotsi, *Energy Environ. Sci.*, 2014, **7**, 867–884.
33 G. Nystrom, A. Marais, E. Karabulut, L. Wagberg, Y. Cui and M. M. Hamedi, *Nat. Commun.*, 2015, **6**, 7259.
34 M. Beidaghi, W. Chen and C. Wang, *J. Power Sources*, 2011, **196**, 2403–2409.
35 K. Sun, T.-S. Wei, B. Y. Ahn, J. Y. Seo, S. J. Dillon and J. A. Lewis, *Adv. Mater.*, 2013, **25**, 4539–4543.
36 W. Sun, R. Zheng and X. Chen, *J. Power Sources*, 2010, **195**, 7120–7125.
37 M. Hamedi, E. Karabulut, A. Marais, A. Herland, G. Nyström and L. Wågberg, *Angew. Chem., Int. Ed.*, 2013, **52**, 12038–12042.
38 C. P. Rhodes, J. W. Long, K. A. Pettigrew, R. M. Stroud and D. R. Rolison, *Nanoscale*, 2011, **3**, 1731–1740.
39 M. Tebyetekerwa, S. Yang, S. Peng, Z. Xu, W. Shao, D. Pan, S. Ramakrishna and M. Zhu, *Electrochim. Acta*, 2017, **247**, 400–409.
40 M. Zamani, M. P. Prabhakaran and S. Ramakrishna, *Int. J. Nanomed.*, 2013, **8**, 2997–3017.
41 V. Thavasi, G. Singh and S. Ramakrishna, *Energy Environ. Sci.*, 2008, **1**, 205–221.
42 Y.-R. Nian and H. Teng, *J. Electrochem. Soc.*, 2002, **149**, A1008–A1014.

43 P. Taberna, P. Simon and J.-F. Fauvarque, *J. Electrochem. Soc.*, 2003, **150**, A292–A300.
44 T. Chen and L. Dai, *Mater. Today*, 2013, **16**, 272–280.
45 H. Li, J. Wang, Q. Chu, Z. Wang, F. Zhang and S. Wang, *J. Power Sources*, 2009, **190**, 578–586.
46 Y. Shi, L. Peng, Y. Ding, Y. Zhao and G. Yu, *Chem. Soc. Rev.*, 2015, **44**, 6684–6696.